Selective alterations of the host cell architecture upon infection with parvovirus minute virus of mice

Jürg P.F. Nüesch*, Sylvie Lachmann[1], Jean Rommelaere

Program of Applied Tumor Virology, Abteilung F010 and Institut National de la Santé et de la Recherche Médicale U375, Deutsches Krebsforschungszentrum, Heidelberg, Germany

Abstract

During a productive infection, the prototype strain of parvovirus minute virus of mice (MVMp) induces dramatic morphological alterations to the fibroblast host cell A9, resulting in cell lysis and progeny virus release. In order to understand the mechanisms underlying these changes, we characterized the fate of various cytoskeletal filaments and investigated the nuclear/cytoplasmic compartmentalization of infected cells. While most pronounced effects could be seen on micro- and intermediate filaments, manifest in dramatic rearrangements and degradation of filamentous (F-)actin and vimentin structures, only little impact could be seen on microtubules or the nuclear envelope during the entire monitored time of infection. To further analyze the disruption of the cytoskeletal structures, we investigated the viral impact on selective regulatory pathways. Thereby, we found a correlation between microtubule stability and MVM-induced phosphorylation of α/β tubulin. In contrast, disassembly of actin filaments late in infection could be traced back to the disregulation of two F-actin associated proteins gelsolin and Wiscott–Aldrich Syndrome Protein (WASP). Thereby, an increase in the amount of gelsolin, an F-actin severing protein was observed during infection, accounting for the disruption of stress fibers upon infection. Concomitantly, the actin polymerization activity also diminished due to a loss of WASP, the activator protein of the actin polymerization machinery the Arp2/3 complex. No effects could be seen in amount and distribution of other F-actin regulatory factors such as cortactin, cofilin, and profilin. In summary, the selective attack of MVM towards distinct host cell cytoskeletal structures argues for a regulatory feature during infection, rather than a collapse of the host cell as a mere side effect of virus production.
© 2004 Elsevier Inc. All rights reserved.

Keywords: Parvovirus minute virus of mice; Virus induced cytopathic effects; Cytoskeleton; Wiscott–Aldrich Syndrome Protein; Gelsolin; Microtubule stabilization; PKC

Introduction

Autonomous parvovirus MVMp are small icosahedral non-enveloped particles with a single-stranded 5.1 kb linear DNA as a genome. This DNA codes for two structural VP- and at least four non-structural NS-proteins. Among the non-structural regulatory proteins, only the large 83-kDa polypeptide NS1 is essential for a productive infection, while the three 24-kDa NS2 proteins are dispensable in permissive non-murine cells. During a productive infection in mouse fibroblast A9 cells, MVMp undergoes a lytic cycle for propagation and spreading (for review, see Cotmore and Tattersall, 1987).

For canine parvovirus, CPV virus entry has been described in great detail. After attachment to the transferrin receptor, the non-enveloped particles are internalized and transported through clathrin-coated pits along the microtubules to the nucleus (Suikkanen et al., 2003a,b; Vihinen-Ranta et al., 2000). During the endosomal transport, partial decapsidation occurs through acidification-dependent pro-

---

* Corresponding author. Program of Applied Tumor Virology, Abt. F010 and INSERM U375, Deutsches Krebsforschungszentrum, Im Neuenheimer Feld 242, D-69120 Heidelberg, Germany. Fax: +49 6221 424962.

E-mail address: jpf.nuesch@dkfz-heidelberg.de (J.P.F. Nüesch).

[1] Present address: Protein Phosphorylation Laboratory, Cancer Research UK, London, United Kingdom.

teolytic cleavages. Thereby, conformational alterations are induced, in which the N-terminal domain of VP1 becomes exposed outside of the spherical capsid (Cotmore et al., 1999). This exposed N-terminal VP1 domain seems to be crucial for the establishment of a productive infection, since it exerts a novel viral PLA$_2$-activity (Zadori et al., 2001). In addition to this enzymatic activity, this part of the large structural protein contains clusters of basic motifs, which could contribute to nuclear import of the viral DNA (Lombardo et al., 2002). Although the receptor is still unknown, MVM entry seems to be similar to CPV. Viral particles are also transported through endosomes, where partial uncoating is achieved by acidification-dependent proteolysis (Ros and Kempf, 2004; Ros et al., 2002).

Once in the nucleus the single-stranded genome of autonomous parvoviruses is converted to a covalently closed circle in a cyclin A-dependent way during cellular S-phase (Bashir et al., 2000). The so-called monomer duplex intermediate serves as a template for RNA-transcription in order to generate the viral (NS-)proteins. All further steps, including DNA-amplification, capsid protein production, and packaging are dependent on the presence of the multifunctional viral phosphoprotein NS1. It is required for viral DNA amplification and *trans* activation of the P38 promoter driving capsid gene expression. Furthermore, it constitutes the major cytotoxic component due to its interference with the host cell physiology and morphology (Anouja et al., 1997; Corbau et al., 2000). Besides its ability to form oligomers (Nüesch and Tattersall, 1993; Pujol et al., 1997), NS1 has been found to interact with a variety of cellular proteins. Such interactions with host cell factors were shown to be necessary for viral DNA amplification (Christensen and Tattersall, 2002) and transcriptional regulation (Krady and Ward, 1995; Lorson et al., 1998), but may also fulfill other as yet unknown functions during infection (Cziepluch et al., 1998). For all these different tasks, NS1 is at least in part regulated by phosphorylation in a timely coordinated manner (Corbau et al., 1999, 2000; Daeffler et al., 2003; Nüesch et al., 1998b), which alters the biochemical profile of the polypeptide (Nüesch et al., 1998a, 2001). This is achieved by serine/threonine kinases, of which members of the PKC family, in particular, PKCλ and PKCη, have been identified as regulators of the NS1 functions necessary for viral DNA amplification in vitro and in vivo (Dettwiler et al., 1999; Lachmann et al., 2003; Nüesch et al., 2003). Interestingly, MVM is not only a target for cellular protein kinases but appears to modulate corresponding signaling pathways (Anouja et al., 1997; Lachmann et al., 2003; Nüesch et al., 2003).

In addition to NS1, the small regulatory NS2 proteins are able to influence the cellular environment as well, although they are dispensable in certain cell types and no enzymatic activities have been attributed to these polypeptides so far. NS2 was shown to interact physically with members of the 14-3-3 family of proteins (Brockhaus et al., 1996) and the nuclear export factor Crm1 (Bodendorf et al., 1999). The latter interaction regulates the export of capsids from the nucleus into the cytoplasm (Eichwald et al., 2002; Miller and Pintel, 2002). On its own, the NS2 functions seem to be well tolerated by the host cell (Mousset et al., 1994). In combination with the NS1 protein, however, the host cell suffers from increased cytotoxicity (Brandenburger et al., 1990). Whether this effect is due to a synergistic action of NS1 and NS2 or represents a mode of regulation of the cytotoxic effector NS1 is presently unclear.

The mechanisms of NS1 induced cytotoxicity as well as viral functions leading to cell death, cytolysis, and release of infectious progeny particles are largely obscure. Remarkably, MVMp infection of A9 cells leads to characteristic alterations of the host cell morphology prior to cell lysis, which may facilitate release of progeny particles into the medium. Early during infection, sub-nuclear structures termed APAR bodies are formed, which serve as replication centers for viral DNA amplification (Bashir et al., 2001; Cziepluch et al., 2000). At later time-points, probably due to size enlargement, these APAR bodies appear to fuse with other subnuclear structures, such as Cajal-, PML-, and speckled bodies (Young et al., 2002a,b). In addition, MVM also induces significant changes within the cytoplasm of infected cells, leading to a collapse of the whole cytoplasm, rounding-up the infected cell and detachment from the culture dish prior to cytolysis (Caillet-Fauquet et al., 1990). Although attributed to the activity of NS1 (Corbau et al., 2000), the nature, functions, and mechanisms of these cytopathic effects are presently unknown.

The present study was undertaken to determine the impact and triggers of MVM on the host cell morphology, particularly the nuclear/cytoplasmic compartmentalization and the cytoskeletal filaments. These analyses revealed that the nuclear entity remains intact throughout the infectious cycle, arguing for the importance of this subcellular compartmentalization for progeny particle production. Moreover, while micro- and intermediate filaments such as actin and vimentin are subject to rearrangements and degradation in the course of infection, microtubules remain largely unaffected. The selective destruction of actin filaments correlates with the concomitant induction of the actin-severing protein gelsolin together with a loss of the polymerization factor WASP. In contrast, the microtubule network seems to be actively protected as a result of MVM infection as apparent by the resistance towards nocodazole treatment and gain of a tubulin-specific phosphorylation. We also provide data that indicate a role for atypical PKCλ not only in the regulation of actin stress fibers (Uberall et al., 1999) but also of microtubules. Altogether, our results suggest that the morphological alterations induced upon MVMp infection of A9 cells represent regulated

processes rather than non-specific side-effects of progeny particle production.

Results

Impact of MVM on nuclear/cytoplasmic compartmentalization of infected cells

A productive MVMp infection is characterized by induction of strong morphological alterations culminating in cytolysis of its host cell (Cotmore and Tattersall, 1987). As shown in Fig. 1, A9 cells asynchronously grown on spot-slides were infected with 30 pfu/cell of MVMp and monitored over a 2-day period by phase-contrast micro-scopy and immunofluorescence using anti-MVM capsid antibodies. Up to 24 h post-infection, the cellular integrity remains largely unaffected by MVMp, presenting the characteristic star-like shape of these fibroblasts and a distinct separation of nuclear and cytoplasmic compart-ments. At later stages of infection as shown 48 h p.i., the majority of the infected cells changed their overall shape. While some cells induced large protrusions, a significant proportion of the population became rounded-up or dis-appeared from the culture either by detachment from the culture dish surface or by cell lysis induced at this stage of infection (Daeffler et al., 2003). Although nuclei and cytoplasm of some cells significantly lost in size, the two cellular compartments were here still distinguishable.

In contrast to MVMp other virus/cell systems such as cytomegalovirus (Muranyi et al., 2002), infection destroys the nuclear/cytoplasmic compartmentalization. Therefore, we analyzed in more detail the nuclear lamina of infected and non-infected A9 cells by immunofluorescence and biochemical fractionations. Asynchronously growing A9 cells seeded on spot-slides were infected with 30 pfu/cell of MVMp fixed in paraformaldehyde 24 and 48 h post-

infection and analyzed in comparison to non-infected cells by immunofluorescence staining with specific antibodies recognizing lamin B and rhodamine-coupled phalloidin. As shown in Fig. 2, the nuclear compartment remained indeed intact, even as late as 48 h p.i., when a significant proportion of infected cells (>50% of the cell population) were rounded-up as apparent from rhodamine-phalloidin staining (marked by arrowheads). To further substantiate these data, we performed biochemical solubility fractionation of whole cell populations. The structure (rigidness) of the lamin B filaments was determined by stepwise extraction of whole cell lysates with increasing amounts of detergents. The amount of lamin B in individual fractions was then quantified by Western blotting. Fraction 1 contains all soluble proteins in absence of any detergents, while fractions 2–4 comprised the proteins whose solubilization required 0.5% CHAPS, 0.5% CHAPS/0.2% deoxycholate, and 0.5% CHAPS/0.2% deoxycholate/0.1% SDS, respec-tively. Fraction 5 contains the remainder components released from the insoluble pellet by heating at 100 °C in Laemmli-buffer. As shown in Fig. 3A, the solubility of lamin B proteins remained unchanged upon MVM infec-tion. In agreement with the current model for the dynamics of cytoskeletal filaments (Pollard et al., 2001), it can be concluded that the lamin filament structure of A9 cells is mainly present in the form of a rigid stable network, as apparent from the mainly detergent resistant protein pool, while soluble lamin B monomers and dimers are absent. Altogether, these results strongly suggest that nuclear/cytoplasmic compartmentalization remains intact through-out the infection at least until cytolysis occurs.

The integrity of the nuclear envelope during a MVM infection was analyzed in regard to the presence and association of two nuclear pore complex proteins, NUP62 and NUP88. A biochemical fractionation procedure based on both sedimentation and solubility of subcellular struc-tures was used which allows the determination of the
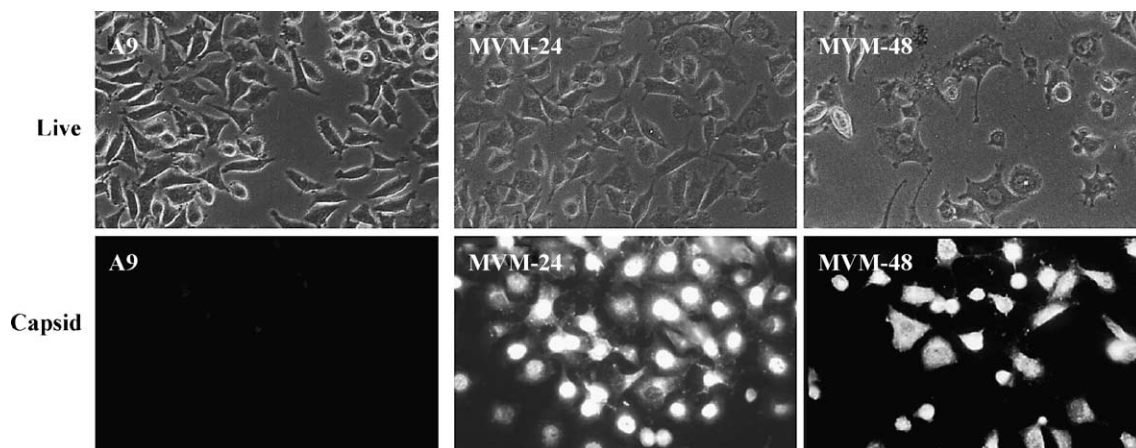

Fig. 1. Determination of MVMp-induced cytopathic effects and release of progeny virus particles. Asynchronously growing A9 cells were infected or not with MVMp (30 pfu/cell). Upper panel: phase-contrast pictures were taken from living cultures at 24 h and 48 h post-infection. Lower panel: cells grown on spot-slides were fixed with paraformaldehyde at 24 and 48 h p.i. and analyzed by immunofluorescence using a mixture of two mouse monoclonal anti-capsid antibodies (EIIF3 and 3D9) and Cy2-conjugated anti-mouse IgG.
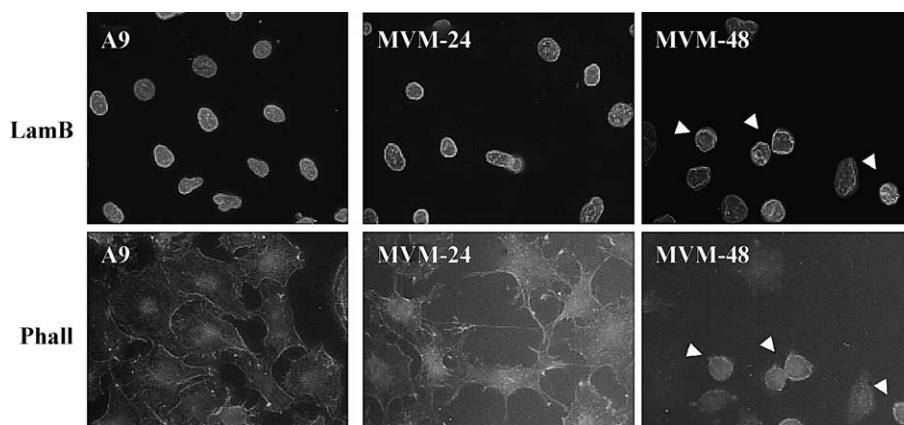
Fig. 2. Immunofluorescence analysis of the nuclear envelope integrity in MVMp-infected A9 cells. A9 cells grown on spot-slides were infected or not with MVMp (30 pfu/cell) incubated for 24 or 48 h, and fixed using paraformaldehyde. Upper panel: the nuclear envelope was visualized by immunofluorescence using a goat polyclonal antiserum raised against lamin B and Cy2-conjugated anti-goat IgG (LamB). Lower panel: cells were counterstained using rhodamine-coupled phalloidine in order to reveal morphological changes induced by MVM. Immunofluorescence staining for the viral NS1 protein at 48 h p.i. showed that over 90% of the cell population was infected with MVMp (data not shown). Rounded-up cells 48 h p.i. are marked by arrowheads.

incorporation of polypeptides within membrane and/or filamentous structures (Lehel et al., 1995). Thus, A9 cells, infected or not with MVMp, were homogenized subsequently and the insoluble material was then separated from the cytosolic fraction by low-speed centrifugation. This insoluble part of the cell lysate revealed the insoluble scaffold components (iS) and mainly the nuclear membrane proteins (nM). The cytosolic components present in the supernatant were also fractionated into soluble cytosolic proteins (C), the cytoplasmic scaffold proteins (sS), and the polypeptides connected to small (mostly postnuclear) membrane structures (pM). Although such a fractionation

procedure does not allow the identification of distinct cell compartments, it is suitable to monitor changes in subcellular structures and the association of proteins with such microdomains. As shown in Fig. 3B, fractionation of A9 cells and consecutive Western blotting revealed about half of the total amount of NUP62 as a soluble protein (C), whereas most of the remaining part remained strongly associated with the insoluble scaffold (iS). While no apparent changes were detected in the distribution of NUP62 upon MVM infection, there was a significant reduction in the overall amount of the protein 48 h p.i., indicating the degradation of this protein. The latter
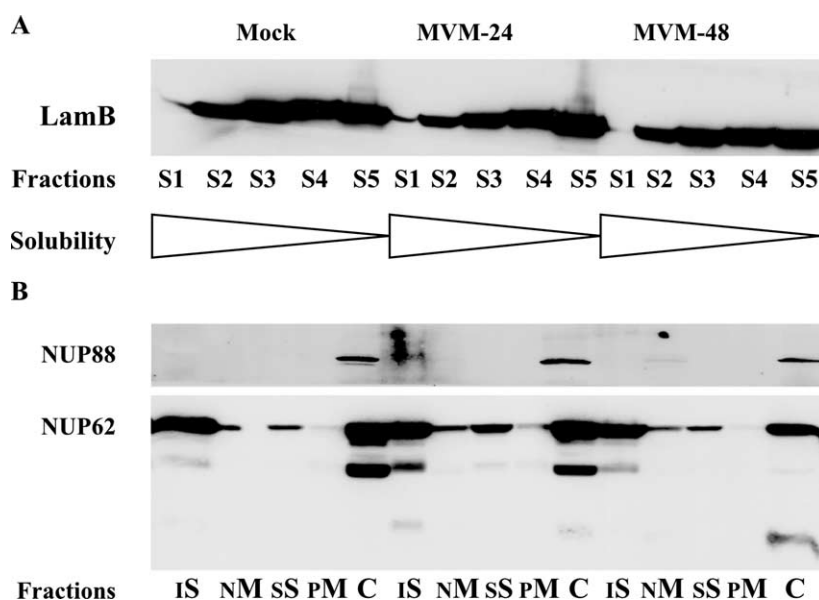

Fig. 3. Biochemical determination of MVMp induced alterations to the nuclear envelope. Asynchronously growing A9 cells were infected or not with MVMp (30 pfu/cell) and harvested at 24 and 48 h p.i. (A) To determine the filamentous structure of nuclear lamin, cellular components were extracted with increasing amount and strength of detergent and the individual fractions (S1 to S5) were analyzed by Western blotting for their lamin B content. (B) Association of nuclear pore proteins with nuclear lamin and/or membrane structures was determined by fractionating cell extracts using a combined sedimentation and Triton X-100 extraction procedure. The distribution of NUP88 and NUP62 proteins in the various fractions was determined by Western blotting. iS, insoluble scaffold; nM, mainly nuclear membranes; sS, soluble scaffold proteins; pM, mainly postnuclear membranes; C, cytosolic soluble proteins.

possibility is supported by the detection of smaller than unit size NUP62 (<62 kDa) in infected cell extracts, which may represent proteolytic cleavage products induced by MVM infection. In contrast to NUP62, the majority of NUP88 was detected as a soluble protein. Interestingly, although a small decrease in the overall amount of NUP88 could be seen 48 h p.i., a small but significant fraction of the polypeptide became associated with "nuclear" membranes. These results indicate that MVM infection can induce specific changes in nuclear pore complex proteins, rather than a general break down of the whole nuclear membrane. A change within the nuclear pore complex might be advantageous for virus release, which is why we measured cell associated progeny virus production and infectious virions released into the medium. The majority of newly produced infectious particles (>50%) remained cell associated throughout the infection (data not shown). Surprisingly, although visible changes in cell morphology and nuclear envelope only occurred 48 h p.i., no significant increase in the proportion of medium released virus became apparent (40% at 24 h p.i. versus 42% 48 h p.i.). Whether these changes are essential to cope with the more than 2-fold increase in total amount of progeny virions produced in the cell population (5×10^7 24 h p.i. versus 1.2×10^8 48 h p.i.), or whether at this time point still other restrictions occur in order to transport progeny virions out of the cell, remains to be determined. Nevertheless, our findings suggest that newly produced MVM virions can be released from the cell by alternative routes than virus-induced cytolysis, although significant changes become visible for the nuclear/cytoplasmic compartmentalization at the end of the cycle.

Selective cytoskeleton alterations induced upon MVMp infection

To identify cytoskeletal structures responsible for the morphological changes of the A9 host cell late in infection (compare Figs. 1 and 2a), we applied immunofluorescence studies. A9 cells grown on spot-slides were synchronized using isoleucine deprivation/aphidicolin treatment, arresting the cells at the G_1/S-border. Isoleucine-depleted cells were infected with 30 pfu/cell MVMp in the presence of aphidicolin, allowing particle uptake, nuclear migration, and decapsidation, but blocking the subsequent step at the level of single-stranded virion DNA conversion to a monomer duplex. Infected cultures were then released into the cell cycle, allowing the viral cycle to resume and proceed in a synchronized fashion. Cells were fixed after 6, 10, 14, 25, and 36 h post-release, and analyzed by immunofluorescence for the respective cytoskeleton filaments (using rhodamine-coupled phalloidin for the microfilament actin, anti-vimentin for intermediate filaments, and anti-tubulin α for microtubules). To identify infected cells proceeding into the virus cycle, we additionally stained for the presence of NS1 using anti-NS1$_C$. Uninfected synchronized S-phase cells (10 h p.r.) served as negative controls. As

shown in Fig. 4 (NS1), the great majority of infected cells proceeded with virus replication. (i) Most pronounced effects that could be attributed for the morphological differences upon MVM infection were seen for the microfilaments (Fig. 4A, actin). As early as 10 h, post-release actin fibers become degraded, and phalloidin-interacting components start to accumulate in "patches" until the cytoplasm collapsed and the cells rounded up (36 h p.r.). (ii) Intermediate filaments are among the most rigid structures and usually responsible for the morphological appearance of eukaryotic cells. Besides forming a regular network, vimentin normally accumulates in a large strand spanning from one end to the other of an A9 fibroblast (Fig. 4A, Vim). Starting at 10 h p.r., these large structures become re-arranged, accumulating around the nucleus by 14 to 25 h p.r. (arrow heads) before the network collapses. Interestingly, in spite of this reduction of vimentin staining at the cell periphery, the general appearance of infected cells 25 h p.r. remained rather normal, similar to that of the cell population monitored 10 p.r. (iii) In contrast to micro- and intermediate filaments, MVM infection had little impact on microtubules, which persisted and formed a network on the cell shape (Fig. 4A, Tubα).

It should be mentioned that similar immunofluorescence experiments were carried out upon MVMp infection of asynchronously grown A9 (data not shown) and permissive human NB324K cells. As illustrated in Fig. 4B, the cytoskeletal changes described above were also observed under these conditions, demonstrating that these structural alterations were not due to the synchronization procedure and were not just specific for A9 cells. Thus, MVMp-infected NB324K cells kept their microtubule network (Fig. 4B, Tubα), displayed the characteristic patching reorganization of actin filaments (Fig. 4B, Actin) and degradation of vimentin fibers (Fig. 4B, Vim). It is noteworthy that contrary to A9 cells, infected NB324K cells failed to show the transient perinuclear accumulation of vimentin, suggesting that this feature is a mere consequence of collapsing rather than of new filament formation.

Cytoskeletal filaments are dynamic structures depending on an equilibrium between polymerization/nucleation and depolymerization/severing events. In order to determine possible disregulations upon infection, we also performed biochemical fractionations according to the solubility of the individual cytoskeleton components. As described for lamin B (Fig. 3), infected and non-infected A9 cells were extracted with increasing amount of detergents and analyzed by Western blotting. As shown in Fig. 5 (Actin and Vim panel), micro- and intermediate filaments were subject to degradation upon MVM infection of A9 cells, resulting in a significant loss of detergent-resistant components. In contrast, fractionation of microtubules showed little differences between MVM-infected and non-infected A9 cells (Fig. 5, Tubα panel). In summary, MVM infection leads to selective rearrangements and degradation of cytoskeleton filaments, which are likely to account for
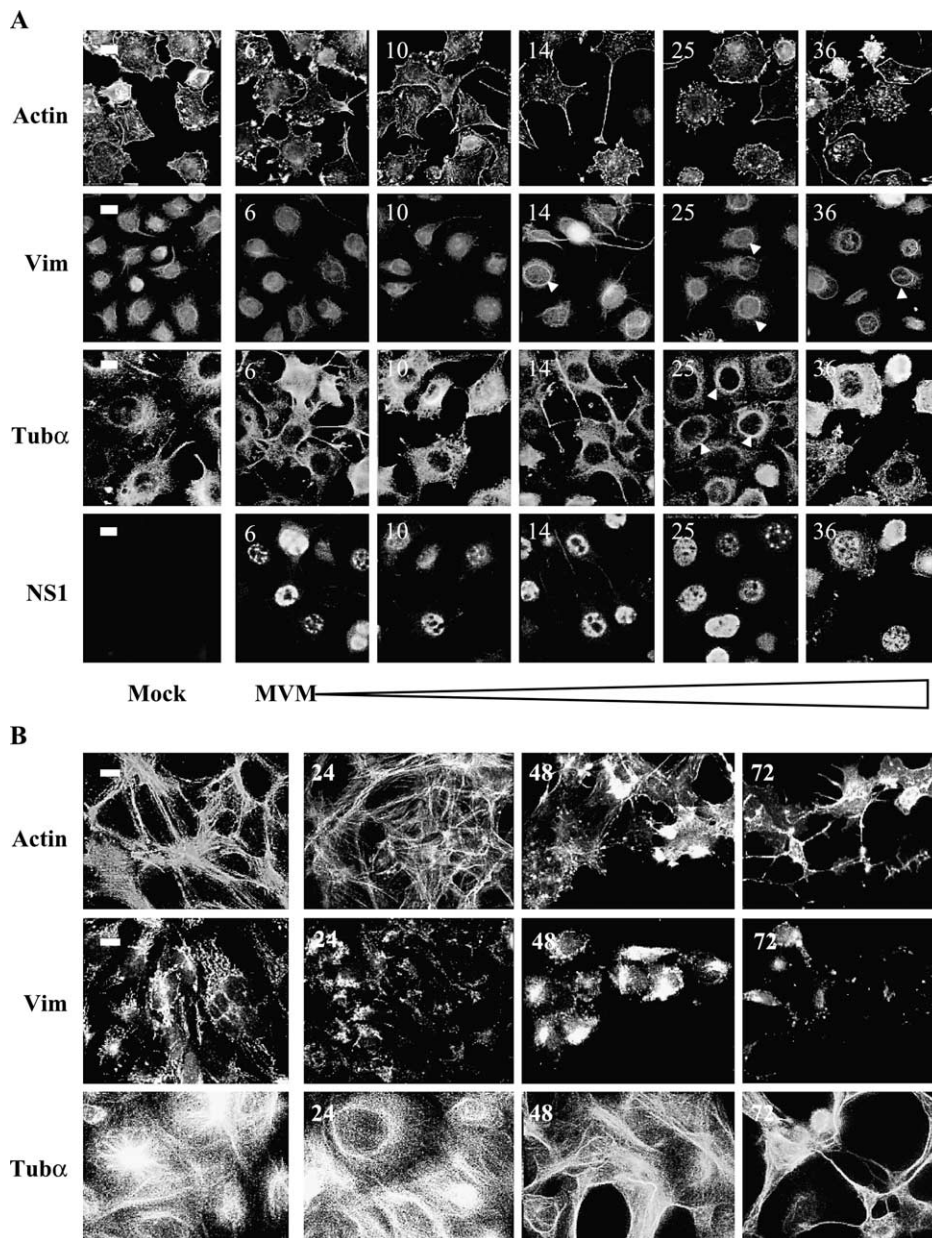
Fig. 4. Determination of alterations to distinct cytoskeleton filaments induced by autonomous parvovirus MVMp. (A) A9 cells grown on spot-slides were arrested at the G1/S-phase border, infected (or not) with MVMp (30 pfu/cell), and released into the cell cycle, allowing virus replication to proceed. Cultures were fixed with paraformaldehyde at 6, 10, 14, 25, and 36 h post-release, and analyzed by immunofluorescence for actin filaments (using rhodamine-coupled phalloidine), intermediate filaments (using a goat polyclonal antiserum raised against vimentin and FITC-coupled anti-goat IgG), and microtubules (using mouse monoclonal antibodies raised against tubulin α). The proportion of MVM-infected cells was determined by immunostaining for the viral NS1 protein (using a polyclonal rabbit antiserum raised against the C-terminal 16 amino acids of this protein and FITC-coupled anti-rabbit IgG) together with immunostaining for microtubules. The characteristic cytoskeletal ring-structures induced upon MVM infection are marked with arrowheads. (B) Asynchronously growing NB324K cells were infected with MVMp (30 pfu/cell) fixed 24, 48, and 72 h p.i. and analyzed for actin-filaments, vimentin, and microtubules as mentioned above. Immunostaining of NS1 showed that over 90% of the cell population was infected with MVM (data not shown).

the morphological alterations imposed to the host cell. Major changes were observed for micro- and intermediate filaments, while microtubules remain largely unaffected. These data give evidence to suggest that the morphological alterations of MVM-infected cells result from a viral interference with distinct cellular processes regulating the cytoskeleton dynamics rather than being mere side-effects of virus replication.

Regulation of actin filament dynamics during MVM infection

Rearrangement of actin filaments to accumulate into "patches" seem to be general features observed in both MVM-infected murine and human cells. Therefore, it was of interest to determine mechanisms leading to these microfilament alterations. To identify actin-regulating proteins
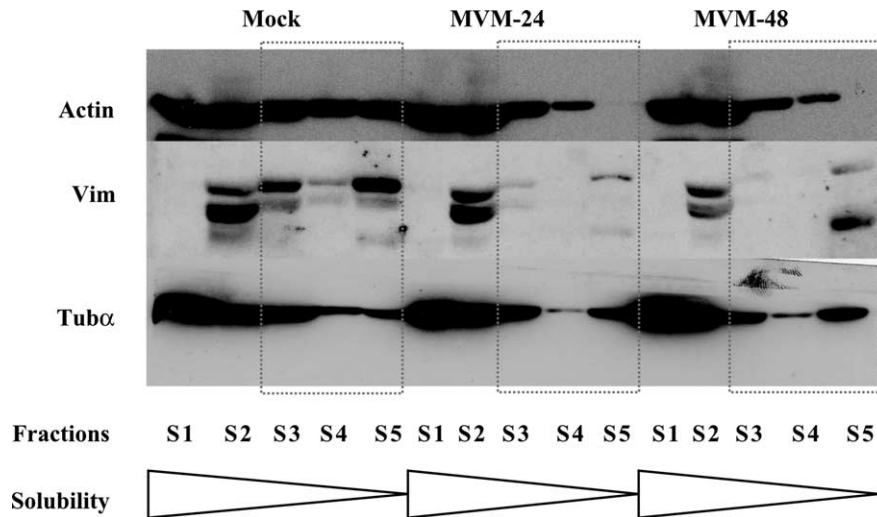
Fig. 5. Biochemical determination of MVMp induced alterations to cytoskeleton filaments. Asynchronously growing A9 cells were infected with MVMp (30 pfu/cell), harvested 24 and 48 h p.i. and analyzed for the solubility of their cytoskeleton filaments. Cell extracts were treated with increasing amounts and strength of detergents (see Fig. 3, upper panel), and the individual fractions (S1 to S5) were analyzed for actin, vimentin, and tubulin α content by Western blotting.

that are target for MVM induced actin restructuring, we performed biochemical fractionations of infected and non-infected cell extracts according to sedimentation and the solubility of subcellular compartments as previously established to monitor NUP62 and NUP88 (see Fig. 3). The following proteins known for their involvement in filamentous (F-)actin metabolism were investigated for MVM induced alterations: (a) *profilin*, an actin-monomer binding protein serving as adaptor with the Arp2/3 complex and activates polymerization at the plasma membrane; (b) *cortactin*, an F-actin-binding protein regulating branching; (c) the actin-depolymerizing factor *cofilin*; (d) the actin-

severing and capping protein *gelsolin*; and (e) Wiscott–Aldrich Syndrome Protein (WASP) an activator of the Arp2/3 complex, the actin polymerization machinery. As shown in Fig. 6, no significant changes could be seen for profilin, cortactin, and cofilin upon MVM infection. In contrast, both the amount and distribution of WASP and gelsolin became altered. While gelsolin, a negative regulator of F-actin formation became induced upon MVM infection, the amount of the activator WASP gradually diminished with time. Interestingly, although the overall amount of WASP decreased in infected cells, a significant proportion became associated to the "nM-Fraction". Likewise, gelsolin increas-
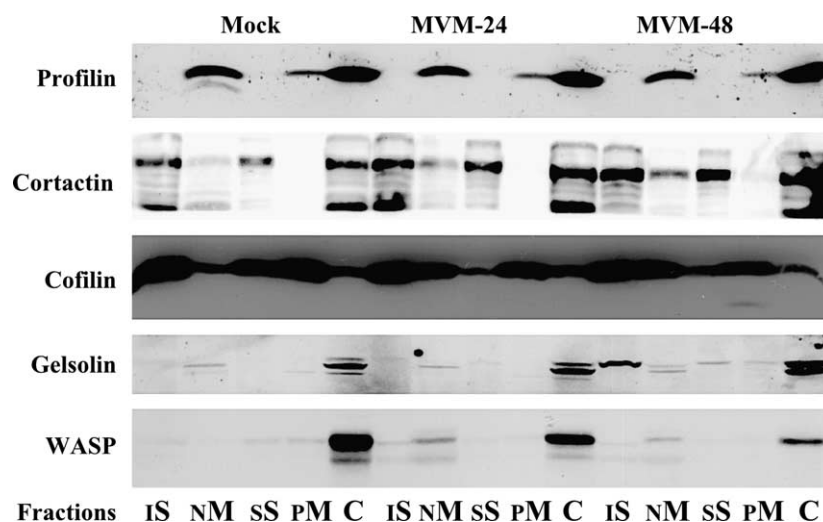

Fig. 6. Changes in the actin polymerization/severing machinery induced upon MVMp infection of A9 cells. Asynchronously growing A9 cells were infected or not with MVMp (30 pfu/cell) and harvested 24 and 48 h p.i. Infection was tested for its impact expression of distinct components/regulators of the actin polymerization and severing machinery and their association with cytoskeleton filaments and/or membrane structures. Cell extracts were prepared and fractionated as described in the legend to Fig. 3 (lower panel). The distribution of profilin, cortactin, cofilin, gelsolin, and the Wiscott–Aldrich Syndrome Protein (WASP) within the various fractions was determined by Western blotting. iS, insoluble scaffold; nM, nuclear membranes; sS, soluble scaffold; pM, post-nuclear membranes; C, cytosol.

ingly became associated with the "iS-" and "nM-fractions". These data indicate that not only the rate of polymerization was affected upon infection, but also the location of F-actin processing may be influenced by the presence of viral proteins. Moreover, the variations of gelsolin mobility in SDS-gels points to possible post-translational modifications of this protein during infection. Altogether, the WASP and gelsolin alterations strongly suggest that MVM infection influences the cytoskeleton dynamics by interfering with (F-actin) regulatory proteins.

The microtubule network is actively protected during MVM infection

Although the individual cytoskeleton filaments are independent structural elements, a "selective" destruction of one filament structure, for example, F-actin often affects other filaments as well. Therefore, it was remarkable that the MVM-induced destruction of F-actin stress-fibers had only little impact on the microtubule network of infected cells. In this respect, it was of interest to determine whether or not microtubules become actively stabilized upon infection and henceforth protect these filaments from collapsing as a consequence of the micro- and intermediate filament destruction.

At first, we determined whether MVM was indeed able to actively protect microtubules from degradation. In the presence of nocodazole, an inhibitor of tubulin GTPase activity, microtubules become destabilized with time. Therefore, we treated both MVM-infected (16 h p.i.) and non-infected A9 cells for 8 h with 100 μM nocodazol. Cells were harvested, and the extracts were fractionated according to their solubility using increasing amounts and strength of detergents as previously described. The distribution of tubulin α in the different fractions was then quantified by Western blotting. As shown in Fig. 7A (lanes 1 and 2), nocodazole significantly reduced the most insoluble tubulin α present in fractions S4 and S5 from non-infected A9 cell extracts. In contrast, MVM-infected cells still contained large amounts of detergent-resistant tubulin α, indicating that MVM infection induces specific protection of the microtubule network against (drug-induced) destabilization.

Such protection could likely be achieved through posttranslational modifications, such as phosphorylation. Two possibilities are to be considered. Modification of the filaments could directly stabilize the network. On the other hand, factors regulating the dynamics of polymerization and depolymerization could be targets tipping the balance towards filament formation. Previously, MVM was shown to influence the cellular physiology by interfering with signaling cascades (Lachmann et al., 2003; Nüesch et al., 2003) leading to alterations in the phosphorylation of cellular proteins (Anouja et al., 1997). This led us to investigate in more detail the effect of MVM infection on tubulin phosphorylation.

PKCλ-mediated protection of microtubules during MVM infection

It was shown that distinct PKC isoforms become redistributed within the cell upon MVM infection (Lachmann et al., 2003; Nüesch et al., 2003) and atypical PKC present in a complex together with CDC42 seem to be involved in the control of polarized microtubule formation during cell migration (Henrique and Schweisguth, 2003). These data led us to investigate whether MVM affected the stability of the microtubule network through phosphorylation by PKC. In that case, stabilization of microtubules should be reduced under conditions that block activation of PKC. To inhibit PKC activity in the target A9 fibroblast cell line, we generated a stably transfected derivative expressing a dominant-negative mutant (K204M) form of the PKC activator PDK-1 under the control of the MVM NS1-inducible P38 promoter (A9:P38-PDKdn). This approach for modulating endogenous protein kinase activity has been used previously in order to analyze the effects of PKCη-driven phosphorylation on MVM DNA replication in vivo (Lachmann et al., 2003). It is noteworthy that a basal expression level of the transgene is sufficient to modulate the target protein kinase already under non-induced conditions (i.e., in absence of MVM NS1). Thus, the A9:P38-PDK:K204M cell line shows an overall reduced PKC activity, which is further downregulated upon MVM infection (Nüesch unpublished results). As shown in Fig. 7A (lanes 3–6), inhibition of PDK-1 resulted in a reduction of insoluble microtubules (S4 and S5 fractions) to similar (Mock) or even greater (MVM) extent as compared with nocodazole treatment. These data would be consistent with a role of PDK-1 in both microtubule networking (lanes 1 vs. 3, mock) and MVM-induced microtubule stabilization (lane 3, Mock vs. MVM).

To study the effects of distinct PKC isoforms on the microtubule filament network, we then transferred a second construct into this cell line, expressing the appropriate constitutive-active PKC variant under the control of the parvoviral P38 promoter. Either of three PKCs were used to this end: the NS1-regulating kinases PKCλ:A119E, and PKCηA160E, these isoforms become activated upon MVM infection (Lachmann et al., 2003; Nüesch et al., 2003) and PKCζA111E due to its structural and functional similarity with PKCλ. The resulting double transfectants were named A9:P38-PDKdn + λca, A9:P38-PDKdn + ζca, and A9:P38-PDKdn + ηca. All cell lines had similar growth rates and were able to support MVM gene expression as determined by immunofluorescence of NS1 (data not shown). To test for an involvement of these PKC isoforms, we further analyzed the microtubule network in these double-transfected cell lines described above by fractionations. No significant increase of insoluble tubulin α was detected in A9:P38-PDKdn cell lines complemented with constitutive-active PKCη or PKCζ, irrespective of MVM infection (Fig. 7A lanes 5
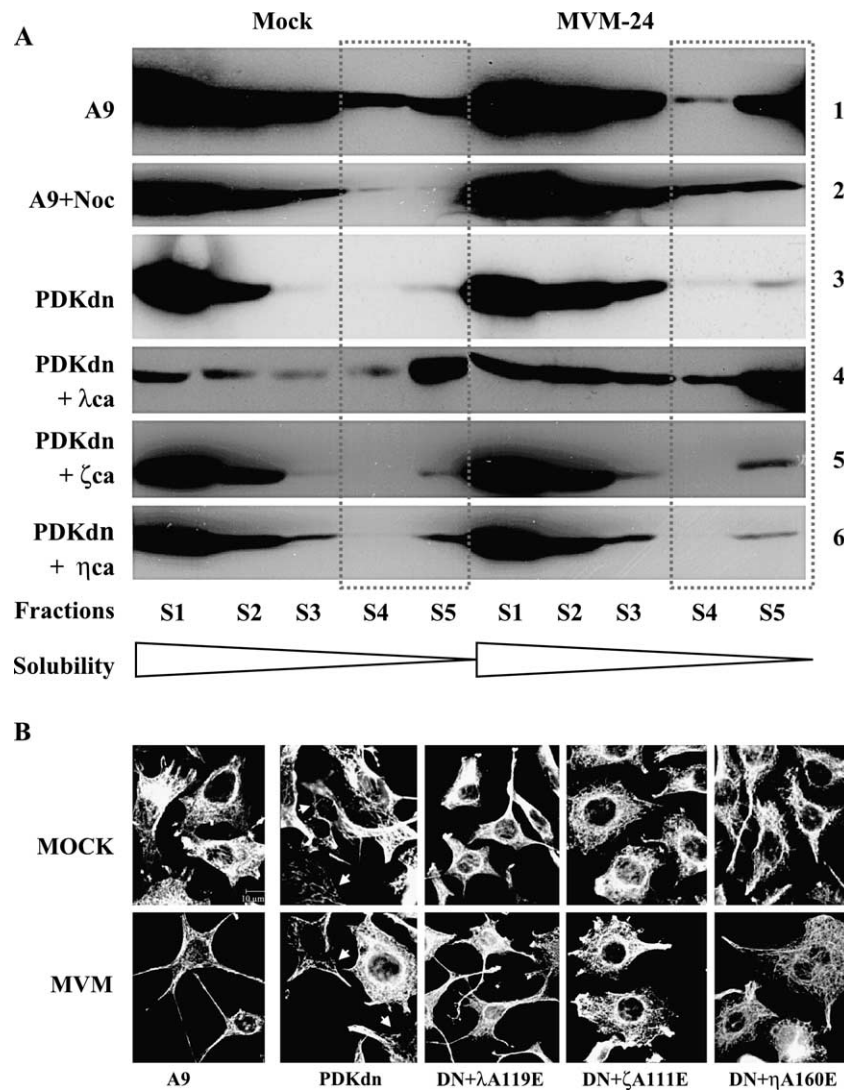
Fig. 7. Impact of PKCλ on microtubule stability. Asynchronously growing A9 cells or derivatives thereof (A9-P38:PDKdn, A9-P38:PDKdn + λca, A9-P38:PDKdn + ηca, A9-P38:PDKdn + ζca) were infected or not with MVMp (30 pfu/cell) and incubated for 24 h. When applied, 100 μM nocodazole was given during the last 6 h of this incubation. (A) Solubility of tubuline. Cells were harvested and proteins were extracted with increasing amounts and strength of detergents as described for lamin B (Fig. 3, upper panel) and the distribution of tubulin α in the various fractions was measured by Western blotting. Detergent-resistant fractions S4 and S5 are framed. (B) Cells grown on spot-slides were fixed with paraformaldehyde and the microtubule network was visualized by immunofluorescence using a mouse monoclonal antibody raised against tubulinα and Cy3-conjugated anti-mouse IgG. Over 90% of the infected cell population showed positive staining for the viral NS1 protein (data not shown).

and 6 vs. lane 3), suggesting that these PKC isoforms do not play a major role in microtubule network formation in A9 cells. In contrast, a remarkable rescue of insoluble tubuline α (S5-fraction) could be observed in extracts from both non-infected and MVM-infected A9:P38-PDKdn + λca cells (Fig. 7A, lane 4 vs. lanes 1 and 3). Interestingly, although the presence of activated PKCλ increased the most insoluble microtubule fraction, there was also a significant reduction in soluble tubulin α (fractions S1 and S2), likely representing the pool of unassembled tubulin protein. In conclusion, PKCλ could be involved in stabilization of the microtubule network rather than promotion of tubulin assembly in (infected) A9 fibroblasts. For further insight the A9 double cell lines expressing

PDKdn plus constitutive active PKCλ, η, or ζ were also analyzed for tubulin staining by immunofluorescence.

As illustrated in Fig. 7B and in agreement with our fractionation data, expression of a dominant-negative PDK mutant in A9-P38:PDKdn, A9-P38:PDKdn+ηca, and A9-P38:PDKdn + ζca significantly reduced the density of the microtubule network particularly in the periphery of both infected and non-infected cells (arrowheads). This reduction of (insoluble) microtubule filaments had little effect on the overall morphology of uninfected A9 cells, yet it correlated with an inhibition of the induction of long extensions in MVM-infected cells (see also Fig. 4). In contrast with the failure of PKCη and PKCζ to rescue cells from PDKdn-induced alterations, expression of activated

PKCλ in PDKdn-transfectants (A9-P38:PDKdn + λca) had a dramatic impact on both, the overall cell shape as well as microtubule filament network (Fig. 7B, middle panels). Indeed, this cell line was able to develop protrusions, which were particularly prominent after MVM infection as in the case of the parental A9 cells. Moreover, the density of tubulin staining was significantly increased in the presence of PKCλca, with cellular extensions being filled with long rigid microtubule fibers. Together with the fact that MVM infection leads to both a redistribution of endogenous PKCλ (Nüesch et al., 2003) and a protection of microtubules against drug-induced severing, these data strongly suggest that MVM induced activation of PKCλ may prevent the tubulin network from undergoing the degradation inflicted on the other cytoskeleton filaments during infection.

These observations prompted us to investigate whether the protection of microtubules during infection or experimental activation of PKCλ could be correlated with a direct modification of tubulin. Thus, MVM infection of A9 cells was tested for its effect on the phosphorylation pattern of tubulin α/β. Vimentin, an intermediate filament protein, which is known to be regulated through phosphorylation (Inagaki et al., 1996) was also analyzed for the sake of comparison. Thus, A9 cells were infected or not with MVMp (30 pfu/cell) incubated for 20 h and metabolically labeled with ^{32}P-orthophosphate for an additional 4 h period. The ^{32}P-labeled tubulin α/β and the vimentin proteins were isolated separately by immunoprecipitation using specific antibodies and further purified by SDS-PAGE. To identify alterations within the phosphorylation pattern, we performed two-dimensional tryptic phosphopeptide analysis of the purified ^{32}P-labeled proteins. As shown in Fig. 8, the phosphorylation patterns of tubulin in infected and non-infected A9 cells were similar, except for one discrete and prominent phosphopeptide that was induced by MVM (arrowhead). In contrast, no differences in the phosphorylation of vimentin could be detected. Tubulin therefore appears to be a specific target for MVM infection-dependent phosphorylation, correlating with the selective protection of this cytoskeleton filament from degradation in infected cells.

Maintenance of an intact microtubule network is essential for progeny virus production in A9 cells

The active maintenance of the microtubule network in MVMp-infected cells raised the possibility that this structure may play a role in efficient progeny virus particle production and/or release. This prompted us to compare the levels of viral DNA amplification and packaging of progeny virion DNA under conditions that preserve or disrupt intact microtubules, respectively. To this end, we took advantage of the A9-derived cell lines described above, differing in the integrity of their microtubule network. Cultures were infected with MVMp (10 pfu/cell) and analyzed 4, 24,
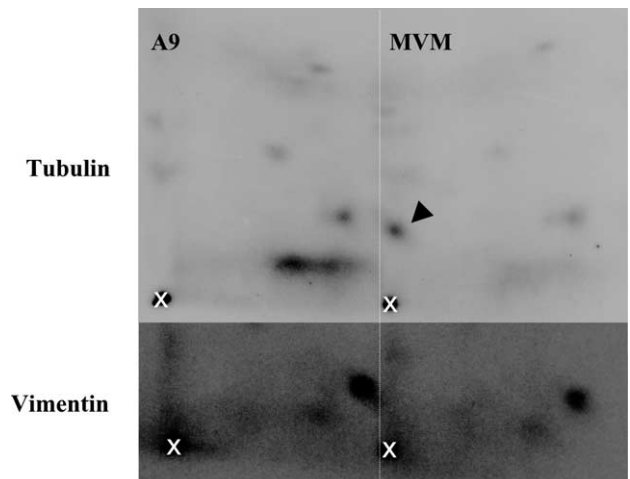

Fig. 8. Phosphorylation pattern of tubulinα/β and vimentin upon MVM infection of A9 cells. Asynchronously growing A9 cells were infected or not with MVMp (30 pfu/cell), metabolically ^{32}P-labeled with orthophosphate for 4 h, and harvested directly into immunoprecipitation buffer. Tubulin α/β and vimentin were isolated by immunoprecipitation, further purified by SDS-PAGE and analyzed for their two-dimensional tryptic phosphopeptide pattern by thin-layer electrophoresis/chromatography. The MVM induced tubulin α/β phosphopeptide is marked with an arrowhead. X marks the loading position.

and 48 h p.i. by Southern blotting for viral DNA amplification formation of monomeric and dimeric double-stranded DNA replication intermediates as well as full progeny particle formation associated with the accumulation of single-stranded virion DNA. All lines were equally efficient in viral uptake as measured by the amount of cell-associated viral ssDNA at 4 h p.i., and the proportion of NS1-expressing cells as determined in parallel by immunofluorescence (data not shown). As shown in Fig. 9, the cell line expressing the dominant-negative mutant form of PDK-1 was impaired in its ability to support viral DNA amplification as compared to the parental A9 cells, although significant amounts of monomeric and dimeric replication intermediates could still be produced. This impairment was most likely due to the reduction of PKC(λ,η) activities necessary to activate the replicative functions of the viral NS1 protein (Lachmann et al., 2003; Nüesch et al., 2003), and could not be overcome by co-expressing individual PKC isoforms. Most interestingly, the production of single-stranded virion DNA could not be detected in the A9-P38:PDKdn, A9-P38:PDKdn + ηca, and A9-P38:PDKdn + ζca lines, but was restored to a very significant extent in the presence of constitutive-active PKCλ (A9-P38:PDKdn + λca). An intriguing correlation could thus be made between progeny virion DNA production and/or packaging on the one hand, and maintenance of the microtubule network on the other hand. Although a cytoskeleton-independent effect of PKCλ, as for instance induction of single-stranded DNA production in order to produce and package progeny virion DNA into preformed capsids cannot be ruled out, these observations led us to speculate that microtubules may facilitate the intracellular transport of viral components, that
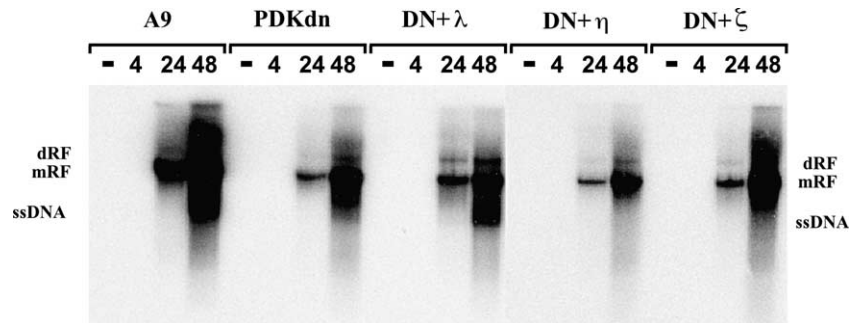
Fig. 9. Determination of MVM DNA replication efficiency in cell lines differing in their PKC and microtubule network status. Asynchronously growing A9 cells or derivatives thereof (A9-P38:PDKdn, A9-P38:PDKdn + λca, A9-P38:PDKdn + ηca, A9-P38:PDKdn + ζca) were infected or not with MVMp (10 pfu/cell). The accumulation of double-stranded replicative forms and single-stranded virion DNA was determined by Southern blotting at 4, 24, and 48 h p.i. dRF, dimer-replicative form; mRF, monomer replicative form; ssDNA, virion DNA. Prolonged exposure showed at 4 h p.i. similar amounts of input ssDNA in infected A9 cells or derivatives (data not shown), indicating that modulation of the PDK/PKC pathway did not affect virus entry.

is, VP-proteins or pre-assembled capsomers/capsids involved in the nuclear formation of infectious virions.

Discussion

The present study shows that the microfilament F-actin and the intermediate filament vimentin get disrupted in A9 mouse fibroblasts upon infection with the autonomous parvovirus MVMp. In contrast, microtubules, which are known to serve as highways for transport to and from the nucleus are maintained throughout the infection. In addition, a hallmark for the eukaryotic cell, the nuclear/cytoplasmic compartmentalization, is not destroyed by MVM, until late in infection when cytolysis occurs. These findings strongly suggest that the virus-induced cytopathic effects result from distinct regulated processes rather than being non-specific consequences of intracellular virus multiplication.

Some of the morphological alterations occurring in virus-infected cells are thought to facilitate virus replication and/or release. In particular, actin modification appears to be an essential feature of the infectious cycle of many viruses, thereby fulfilling various functions. Human cytomegalovirus infectivity depends in part on the ability of this agent to induce the depolymerization of F-actin (Jones et al., 1986). Similarly, Rubella virus causes F-actin disintegration into G-actin aggregates (Bowden et al., 1987). In contrast, a strong induction of actin polymerization is required to propel vaccinia virus particles through the cytoplasm (Cudmore et al., 1995). Actin also regulates the RNP complex of human parainfluenza virus by inducing conformational changes through direct interactions (De et al., 1991). Moreover, actin is found in the capsids of a variety of viruses, for example, HIV-1 (Sasaki et al., 1995) and Rabies virus (Naito and Matsumoto, 1978). By analogy, destruction and rearrangements of selective cytoskeleton filaments induced by MVMp could serve distinct purposes during virus infection as well. MVM-infected cells could be distinguished by a ring-structure surrounding the nucleus and composed of

vimentin (this paper) and tropmyosin (data not shown), as well as by actin patches distributed within the cytoplasm. Though the physiological relevance of these rearrangements is presently unclear, they can be speculated to contribute to intracellular signaling. Indeed it was shown that upon MVM infection, members of the protein kinase C family, particularly the NS1-regulating PKCη become accumulated around the nucleus of infected cells (Lachmann et al., 2003). Knowing that the association of these kinases with the cytoskeleton and membrane structures is involved in their activation make it likely that the perinuclear filamentous ring induced by MVM may influence signal transduction pathways. Likewise, the newly formed patches of polymerized actin may constitute anchors for signaling cascades (Diviani and Scott, 2001).

Alternatively, these islands may be cytoplasmic sites, where virus component become assembled or modified. The MVM-induced production of G-actin through severing of F-actin could be correlated with increased gelsolin and reduced WASP activity in infected cells. These up- and down-modulations could hence be responsible for the MVMp-induced disorganization of the actin network. We are currently investigating whether these actin-regulating factors become modified and/or redistributed in the presence of MVMp, in order to redirect actin-polymerization.

Remarkably, despite severe destruction of micro- and intermediate filaments, the microtubule network showed little alterations in MVMp-infected cells. This appeared to be the result of active protection of microtubules against severing and correlated with an altered phosphorylation pattern of tubulin in infected cells. Microtubules play a central role in intracellular transport mechanisms. In particular, starting from the early stages of parvovirus infection, these filaments are used to shuttle incoming virus to the nucleus, where replication gets established (Suikkanen et al., 2003a; Vihinen-Ranta et al., 2000, 2004). The present work suggests that the integrity of microtubules could be important for later steps during infection as well. Indeed, cell lines in which the microtubule network was disrupted proved to be deficient for

single-stranded virion DNA production. This led us to speculate that microtubules may also be involved in the intracellular trafficking of newly synthesized viral components (e.g., VP-proteins, capsomers and/or (pre)assembled capsids) to the sites of full particle assembly. Microtubules may also contribute to the egress of progeny virions. This hypothesis would be consistent with the present data showing that MVM release is not a mere consequence of cell collapsing and cytolysis.

In contrast to other lytic DNA viruses replicating in the nucleus (Muranyi et al., 2002), MVM does not induce the disruption of the nuclear lamina. This maintenance of the nuclear/cytoplasmic compartmentalization implies that newly produced viral particles have to be transported actively through the nuclear pore into the cytoplasm, a process mediated through direct interaction of the small viral non-structural proteins NS2 with the nuclear export factor crm1 (Eichwald et al., 2002). After crossing, the nuclear membrane progeny virions are likely to be shuttled to the periphery of the cell and released through an active process, since significant amounts of infectious particles were present in the medium already at times when no CPE and cell lysis could be detected (see Fig. 1 and Daeffler et al., 2003). The microtubule network, which seems to be protected from degradation during infection represents a likely candidate for facilitating this active virus secretion.

Our finding that atypical PKCλ is able to protect the microtubule network from degradation is of a particular interest, since it could further underline the central role of PKCs in the regulation of the MVM replication cycle. Thereby, it seems remarkable that like in the case of the multifunctional protein NS1, a few molecules can be (re)programmed by the virus to ascertain an intracellular milieu favoring virus propagation and spread in a highly coordinated way. (i) Previously, we have shown for the NS1 protein that PKCλ phosphorylation at residues T435 and S473 plays a pivotal role, being essential for both, initiation of viral DNA amplification (Dettwiler et al., 1999; Nüesch et al., 2001) and induction of cell alterations leading to cytolysis (Corbau et al., 2000). This apparent conflict was explained by a possible regulation through compartmentalization (Nüesch et al., 2003). Phosphorylation and activation of NS1 by PKCλ for viral DNA amplification occurs in the nucleus at least in the beginning of infection, while major alterations of the host cell morphology apparently occur within the cytoplasm. Therefore, it seems favorable that, as presented in this paper, the nuclear envelope remains intact at least until sufficient progeny particles are produced. A controlled nuclear export of the cytotoxic effector protein NS1 and/or its activator kinase PKCλ, which is endowed with nuclear import and export signals (Perander et al., 2001), would thus allow more confined regulation of NS1-triggered cytoskeleton alterations. Whether such regulation could be mediated through an NS2–crm1 complex is at present

unclear. (ii) The present investigation implies a pivotal role for the PKCλ during MVM infection. Besides activating NS1 for its cytotoxic functions (Corbau et al., 2000), we could show here that the presence of this activated kinase could exert protective effects to the host cell as well.

Although there is a good correlation between MVM-mediated tubulin phosphorylation and the protection of microtubules from drug-induced severing, together with the maintenance of the microtubule network during infection, it remains still speculative whether the experimentally determined impact of PKCλ on microtubule formation indeed occurs during MVM infection. However, an involvement of PKCλ in the regulation of microtubules during MVM infection is further supported by the known role of atypical PKCs in the control of cell polarity. In association with PAR-6, PAR-3, and CDC42, in a complex regulating the cytoskeleton dynamics, atypical PKC were shown to modulate the polymerization of microtubules (Henrique and Schweisguth, 2003). In this regard, it should be stated that in contrast to PKCλ the other atypical PKC isoform, PKCζ was unable to rescue the microtubule network in the presence of a dominant-negative mutant form of PDK-1, suggesting that these two closely related kinases exert different functions in A9 cells as previously implicated by analyzing their subcellular distribution (Nüesch et al., 2003). More detailed analyses, however, will be necessary to determine the molecular basis of PKCλ specificity and to unravel the link between the activation of this kinase, the altered phosphorylation of tubulin α/β, and the protection of the microtubule network that all take place in MVM-infected cells.

Materials and methods

Antibodies and reagents

Antibodies specific for lamin B, vimentin, cortactin, and WASP were purchased from Santa Cruz (M-20, S-20, H-191, B-9), for NUP88, NUP62, and gelsolin from Becton Dickinson (611896, 610497, 810412), for actin from ICN (C4), for tubulin α, tubulin β, and cofilin from Sigma (B-5-1-2, T8535, C8736,), profilin from Alexis (IG706). Rhodamine-conjugated phalloidine was from Molecular Probes (Oregon). Rabbit antisera recognizing the viral non-structural protein NS1 (αNS1$_C$ (Cotmore and Tattersall, 1988)) was previously obtained using specific peptides, while the monoclonal anti-capsid antibodies EIIF3 [kindly provided by Drs. Tattersall and Cotmore], and D3 (Eichwald et al., 2002) were produced with preparations of empty capsids. Horseradish peroxidase (HRP)-conjugated anti-rabbit and anti-mouse antibodies were purchased from Promega, while HRP conjugated anti-goat IgGs were obtained from Santa Cruz. Fluorescent dye-labeled secondary antibodies were from Dianova.

Cells and viruses

A9 fibroblasts, derivatives thereof and NB324K cells were maintained as monolayers in Dulbecco's Modified Eagle Medium (DMEM) containing 10% fetal calf serum (FCS). MVMp was propagated in adherent A9 cells, and virus stocks were prepared by repeated freezing and thawing in 10 mM Tris pH 8.3, 1 mM EDTA. When indicated, full (DNA containing) MVMp particles were purified from empty capsids by CsCl-gradient centrifugation according to their boyant density.

Plasmid constructs

Isolation of mouse PDK-1 cDNA

A9 cDNA libraries were generated from mRNA preparations using a SMART PCR cDNA synthesis KIT (Becton Dickinson, Heidelberg). PDK-1 was cloned by PCR from the mouse fibroblast library in two separate fragments. The N-terminal fragment was obtained using the primer pair A: 5′ -ATGGCCAGGACCACCAGCCAGCTGTATGACG-CTGTGCCCA -3′ , and B: 5′ -TGCCACGAGCTGATAGT-GATACATCCAAGGGCCCAAAGG-3′ for the C-terminal half of the coding region primers C: 5′ -CCTTTGGGCCC-TTGGATGTATAATCTATCAGCTCGTGGCA-3′ , and D: 5′ -TCACTGCACAGCAGCATCTGGATTGCTCTGGT-ACTGCTGC-3′ were used. The two fragments were then combined through the overlapping sequences of primers B and C by additional PCR using primers A and D, and cloned directly into pCR2.1 (Invitrogen). The pCR2.1-PDK-1cDNA was sequenced and showed no differences within the coding sequences was found compared to the Genebank sequences (AF086625).

Production of mutant PDK-1:K204M, PKCλ:A119E and PKCζ:A111E

(i) Site-directed mutagenesis of the mouse PDK-1 cDNA clone was performed by chimeric PCR using the N- and C-terminal primers 5′ -*CCCGGG***ATGGAACAAAAACT-CATCTCAGAAGAGGATCTGAAT**ATGGCCAG-GACCACCAGCCAGCTGTATGACGCTGTGC-3′ and 5′ -TCAGTCTAGACTCGATGCAAAACTGGTGCCA-AGGGTTTC-3′ , together with two overlapping internal primers harboring the mutation. The N-terminal primer includes, besides a unique *Sma*I site (italic) for cloning purposes, the coding sequence for an N-terminal Myc-epitope (bold) in frame with the start codon of the cDNA. The mutated primers used to replace the conserved lysine in the ATP-binding pocket with a methionine were: 5′ -GAATGATGCC-*C***A**TGCCATGCAAGTACTC-3′ and 5′ -GAGTACTTGCA-TGGCA**TG**GGCATCATT-3′ . (ii) Similarly, the constitutive active Flag-tagged PKC mutant *PKCλ:A119E* (replacing alanine to glutamic acid in the pseudosubstrate region) was generated by chimeric PCR with the two mutagenic primers 5′ -CGGAGAGGGG**A**ACGCCGGTGGAGAAAGCTGT-3′ and 5′ -CTCCACCGGCGT**T**CCCCTCTCCGG-TAAATGGAC-3′ using an A9 derived PKCλ cDNA and

Flag-tagged *PKCζ:A111E* (replacing the alanine of the pseudosubstrate site of PKCζ with glutamic acid): 5′ -TACCGCCGGGGGAAG**A**AGATGGAGGAAG-3′ and 5′ -CCATCT**T**CTCTCTCCCCGGCGTGAGATAG-3′ using the full-length human PKCζ cDNA clone (Dettwiler et al., 1999). Flag-tagged PKCηA160E (replacing the conserved alanine in the pseudosubstrate site to a glutamic acid) has been described previously (Lachmann et al., 2003).

Production of expression constructs to generate stably transfected cell lines

MVM NS1-inducible expression vectors were generated from plasmids pP38 or pP38-Flag (Lachmann et al., 2003). The mutant Myc-tagged PDK-1:K204M and PKC clones (see below) were subcloned into pCR2.1 (Invitrogen, Groningen, NL) providing appropriate unique N- and C-terminal restriction sites prior to transfer into the expression vectors. Thus, pP38-MycPDK:K204M and pP38-FlagPKCζA111E were generated by transferring the respective *Sma*I–*Not*I fragments into *Hpa*I–*Not*I-digested pP38, while Flag-PKCλA119E was transferred as an *Eco*47I–*Not*I-fragment into *Eco*47I–*Not*I-digested pP38-Flag. The construction of pP38-FlagPKCηA160E has been described previously (Lachmann et al., 2003).

Generation of stably transfected A9 cell lines

Stable transfectants were generated as previously described by Lachmann et al. (2003). In brief, 10^5 A9 cells or were cotransfected with 25 µg of the appropriate pP38-X construct together with pSV2neo in a molar ratio of 25:1, using 25 µl of Lipofectamine (Invitrogen) according to the manufacturer's protocol. Two days post-transfection, cultures were split 1:10, and transfected cells were selected using 400 µg/ml G418 (SIGMA). Double transfectants were similarly obtained from A9-P38:MycPDK:K204M cells using pTKHyg as a selection marker and 400 µg/ml Hygromycin B. Colonies were pooled after growth for approximately 4 weeks under selection and frozen stocks were prepared. All experiments were performed after additional cell growth for several passages in absence of selection in order to avoid physiological side-effects of G418 or Hygromycin B. To obtain optimal reproducibility, all transfectants were kept in culture for limited times only (less than 25 passages). It should be mentioned that the level of MycPDK:K204M expression in the A9-derivatives was much lower than that of the other transgenes, even under induction with MVM, probably due to the tight dependence of A9 cell survival on PDK-1 activity.

Biochemical fractionation of cellular extracts

Fractionation according to solubility (Karczewski and Strebel, 1996)

Cells were harvested by scraping into the medium, washed repeatedly in PBS. Cell pellets were suspended in

proportional amounts of hypotonic buffer (20 mM HEPES–KOH pH 7.5; 5 mM MgCl$_2$, 5 mM KCl, 1 mM DTT) and proteins were extracted by repeated cycles of freezing and thawing. After incubation for 10 min on ice, soluble proteins (S1) were separated from insoluble material by centrifugation at 15,000 × g for 3 min. S2 was generated by extraction of the insoluble pellet for 5 at room temperature in the same amount of CHAPS-buffer (50 mM Tris pH 8.0, 5 mM EDTA, 100 mM NaCl, 0.5% CHAPS), followed by centrifugation to recover the solubilized components in the supernatant. S3 and S4 fractions were similarly obtained through successive extraction of the insoluble pellet with CHAPS-DOC-buffer (supplemented with 0.2% Na-deoxycholate) and CHAPS-DOC-SDS-buffer (containing 0.1% SDS), respectively. The remaining insoluble pellet was then heated at 100 °C in loading-buffer, before analysis by SDS-PAGE and Western blotting. It should be mentioned at this position that adjusting the fractions to the same volume allowed to compare the amount of the selected proteins proportional to the cell number.

Combined fractionation by sedimentation and Triton X-100 treatment

Cells were processed essentially as described by Lehel et al. (1995). Briefly, cells were harvested by scraping into the medium, washed repeatedly in PBS, and proteins were extracted in hypotonic buffer using a Dounce Homogenizer (tight fitting, 25 strokes) and repeated passing through a syringe (27 gauge). The insoluble material was separated from the soluble fraction by low-speed centrifugation at 800 × g for 5 min at 4 °C. The insoluble pellet was then extracted in hypotonic buffer containing 1% Triton X-100 for 30 min on ice and subjected to centrifugation at 150,000 × g for 1 h, separating the insoluble scaffold proteins (iS fraction) from mostly nuclear membranes in the supernatant (nM-fraction). The soluble components recovered after the first low-speed centrifugation were further fractionated by high-speed centrifugation at 150,000 × g for 1 h. The supernatant containing cytosolic constituents was collected (C-fraction). The pellet was then extracted by incubation in hypotonic buffer containing 1% Triton X-100 for 30 min on ice, followed by high-speed centrifugation segregating the soluble scaffold (sS-fraction) from the postnuclear membranes (pM-fraction) in the supernatant. The pellet fraction was then solubilized in SDS-PAGE loading-dye before Western blotting analysis. As described above for solubility fractionations, the volumes where adjusted to the cell number in order to determine the amount of the selected proteins proportional to the cell number and to monitor redistribution according to the morphological changes induced upon infection.

Western blotting analyses

Protein extracts were fractionated by discontinuous SDS-PAGE and blotted onto nitrocellulose membranes. Proteins of interest were detected by incubation with appropriate primary antibodies in 10% dry milk/PBS for 18 h, and staining with horseradish-peroxidase-conjugated secondary antibodies for 1 h followed by chemiluminescence detection (Amersham).

Immunofluorescence/microscopy

For examination by immunofluorescence microscopy, cells were grown on spot slides, mock- or MVMp-infected and further incubated for appropriate times. Synchronization of A9 cultures were performed by isoleucine deprivation for 44 h followed by an additional incubation for 18 h in complete medium in the presence of 100 μg/ml aphidicolin (Sigma). MVM infection was performed in the presence of aphidicolin. Release of cells into S-phase and concomitant onset of virus replication was induced by extensive washes in DMEM containing 10% FCS. Cultures were then fixed at indicated times post-infection/release using 3% paraformaldehyde in PBS, pH 7.4 for 30 min at room temperature, neutralized with 50 mM NaCl for 6 min and permeabilized by treatment with PBS containing 0.1% Triton X-100 for 10 min. All solutions were supplemented with 1 mM MgCl$_2$ and 0.5 mM CaCl$_2$. After extensive washing, cells were blocked with 10% goat serum for 30 min, incubated with primary antibodies for 2 h at room temperature and stained with FITC-, CY2-, CY3-, or Rhodamine-conjugated anti-species specific antibodies (Dianova). After mounting using Elvanol, cells were analyzed by conventional epifluorescence microscopy (Leica; 63× lens with immersion oil).

NS1 metabolic labeling, purification, and phosphopeptide analyses

Metabolic labeling of NS1 and tryptic phosphopeptide analyses were essentially performed as previously described (Nüesch et al., 1998a). A9 cell cultures (10^7 cells) were infected with MVMp (20 pfu/cell), kept for 24 h before being subjected for 4 h in labeling medium (complete medium lacking phosphate [Gibco/BRL] and supplemented with 0,1 nCi/cell of [^{32}P] orthophosphate [ICN]). Labeled cells were harvested directly in 1 ml of RIPA buffer (20 mM Tris–HCl, pH 7.4, 150 mM NaCl, 1 mM EDTA, 0.1% SDS, 1% Na-deoxycholate, 1% Triton X-100) containing protease and phosphatase inhibitors. NS1 immunoprecipitations were carried out using 10 μl of αNS$_N$ antiserum for 2 h at room temperature. Immune complexes were precipitated with protein A-sepharose, washed with RIPA buffer and further purified by 10% SDS-PAGE. ^{32}P-labeled proteins were revealed by auto-radiography after blotting on polyvinylidene fluoride (PVDF) membranes, and the band corresponding to NS1 was excised. Digestion of membrane bound NS1 was performed with 50 units of trypsin for 18 h at 37 °C. Tryptic peptides contained in the supernatant were recovered by lyophilization and analyzed on thin-layer cellulose

plates (Merck) in two dimensions, first by electrophoresis using a pH 1.9 buffer, and then by chromatography in phosphochromatography buffer.

MVM DNA replication in infected cells

The accumulation of MVM DNA replicative forms was analyzed by Southern blotting as described by (Corbau et al., 1999). A9 cells, 3×10^5 (or derivatives), were infected with MVMp (10 pfu/cell). Cells were harvested in TE-buffer (10 mM Tris–HCl pH 8.0, 1 mM EDTA) at 4, 24, and 48 h post-infection and digested with proteinase K in 0.1% SDS for 18 h at 46 °C. The whole cellular DNA was then sheared by passing through a syringe, fractioned by 0.8% agarose gel electrophoresis, and blotted on a nitrocellulose membrane. Viral replicative intermediates were then detected using a ^{32}P-labeled probe corresponding to nts 385–1885 of the NS1-coding region of MVMp.

Acknowledgments

References

Anouja, F., Wattiez, R., Mousset, S., Caillet-Fauquet, P., 1997. The cytotoxicity of the parvovirus minute virus of mice nonstructural protein NS1 is related to changes in the synthesis and phosphorylation of cell proteins. J. Virol. 71, 4671–4678.

Bashir, T., Horlein, R., Rommelaere, J., Willwand, K., 2000. Cyclin A activates the DNA polymerase delta-dependent elongation machinery in vitro: a parvovirus DNA replication model. Proc. Natl. Acad. Sci. U.S.A. 97, 5522–5527.

Bashir, T., Rommelaere, J., Cziepluch, C., 2001. In vivo accumulation of cyclin A and cellular replication factors in autonomous parvovirus minute virus of mice-associated replication bodies. J. Virol. 75, 4394–4398.

Bodendorf, U., Cziepluch, C., Jauniaux, J.C., Rommelaere, J., Salome, N., 1999. Nuclear export factor CRM1 interacts with nonstructural proteins NS2 from parvovirus minute virus of mice. J. Virol. 73, 7769–7779.

Bowden, D.S., Pedersen, J.S., Toh, B.H., Westaway, E.G., 1987. Distribution by immunofluorescence of viral products and actin-containing cytoskeletal filaments in rubella virus-infected cells. Arch. Virol. 92, 211–219.

Brandenburger, A., Legendre, D., Avalosse, B., Rommelaere, J., 1990. NS-1 and NS-2 proteins may act synergistically in the cytopathogenicity of parvovirus MVMp. Virology 174, 576–584.

Brockhaus, K., Plaza, S., Pintel, D.J., Rommelaere, J., Salome, N., 1996. Nonstructural proteins NS2 of minute virus of mice associate in vivo with 14-3-3 protein family members. J. Virol. 70, 7527–7534.

Caillet-Fauquet, P., Perros, M., Brandenburger, A., Spegelaere, P., Rommelaere, J., 1990. Programmed killing of human cells by means of an inducible clone of parvoviral genes encoding non-structural proteins. EMBO J. 9, 2989–2995.

Christensen, J., Tattersall, P., 2002. Parvovirus initiator protein NS1 and RPA coordinate replication fork progression in a reconstituted DNA replication system. J. Virol. 76, 6518–6531.

Corbau, R., Salome, N., Rommelaere, J., Nüesch, J.P., 1999. Phosphorylation of the viral nonstructural protein NS1 during MVMp infection of A9 cells. Virology 259, 402–415.

Corbau, R., Duverger, V., Rommelaere, J., Nüesch, J.P., 2000. Regulation of MVM NS1 by protein kinase C: impact of mutagenesis at consensus phosphorylation sites on replicative functions and cytopathic effects. Virology 278, 151–167.

Cotmore, S.F., Tattersall, P., 1987. The autonomously replicating parvoviruses of vertebrates. Adv. Virus Res. 33, 91–174.

Cotmore, S.F., Tattersall, P., 1988. The NS-1 polypeptide of minute virus of mice is covalently attached to the 5′ termini of duplex replicative-form DNA and progeny single strands. J. Virol. 62, 851–860.

Cotmore, S.F., D'Abramo Jr., A.M., Ticknor, C.M., Tattersall, P., 1999. Controlled conformational transitions in the MVM virion expose the VP1 N-terminus and viral genome without particle disassembly. Virology 254, 169–181.

Cudmore, S., Cossart, P., Griffiths, G., Way, M., 1995. Actin-based motility of vaccinia virus. Nature 378, 636–638.

Cziepluch, C., Kordes, E., Poirey, R., Grewenig, A., Rommelaere, J., Jauniaux, J.C., 1998. Identification of a novel cellular TPR-containing protein, SGT, that interacts with the nonstructural protein NS1 of parvovirus H-1. J. Virol. 72, 4149–4156.

Cziepluch, C., Lampel, S., Grewenig, A., Grund, C., Lichter, P., Rommelaere, J., 2000. H-1 parvovirus-associated replication bodies: a distinct virus-induced nuclear structure. J. Virol. 74, 4807–4815.

Daeffler, L., Horlein, R., Rommelaere, J., Nüesch, J.P., 2003. Modulation of minute virus of mice cytotoxic activities through site-directed mutagenesis within the NS coding region. J. Virol. 77, 12466–12478.

De, B.P., Lesoon, A., Banerjee, A.K., 1991. Human parainfluenza virus type 3 transcription in vitro: role of cellular actin in mRNA synthesis. J. Virol. 65, 3268–3275.

Dettwiler, S., Rommelaere, J., Nüesch, J.P., 1999. DNA unwinding functions of minute virus of mice NS1 protein are modulated specifically by the lambda isoform of protein kinase C. J. Virol. 73, 7410–7420.

Diviani, D., Scott, J.D., 2001. AKAP signaling complexes at the cytoskeleton. J. Cell Sci. 114, 1431–1437.

Eichwald, V., Daeffler, L., Klein, M., Rommelaere, J., Salome, N., 2002. The NS2 proteins of parvovirus minute virus of mice are required for efficient nuclear egress of progeny virions in mouse cells. J. Virol. 76, 10307–10319.

Henrique, D., Schweisguth, F., 2003. Cell polarity: the ups and downs of the Par6/aPKC complex. Curr. Opin. Genet Dev. 13, 341–350.

Inagaki, M.M.Y., Tsujimura, K., Ando, S., Tokui, T., Takahashi, T., Inagaki, N., 1996. Dynamic property of intermediate filaments: regulation by phosphorylation. BioEssays 18, 481–487.

Jones, N.L., Lewis, J.C., Kilpatrick, B.A., 1986. Cytoskeletal disruption during human cytomegalovirus infection of human lung fibroblasts. Eur. J. Cell Biol. 41, 304–312.

Karczewski, M.K., Strebel, K., 1996. Cytoskeleton association and virion incorporation of the human immunodeficiency virus type 1 Vif protein. J. Virol. 70, 494–507.

Krady, J.K., Ward, D.C., 1995. Transcriptional activation by the parvoviral nonstructural protein NS-1 is mediated via a direct interaction with Sp1. Mol. Cell. Biol. 15, 524–533.

Lachmann, S., Rommeleare, J., Nüesch, J.P., 2003. Novel PKCeta is required to activate replicative functions of the major nonstructural protein NS1 of minute virus of mice. J. Virol. 77, 8048–8060.

Lehel, C., Olah, Z., Jakab, G., Szallasi, Z., Petrovics, G., Harta, G., Blumberg, P.M., Anderson, W.B., 1995. Protein kinase C epsilon subcellular localization domains and proteolytic degradation sites. A model for protein kinase C conformational changes. J. Biol. Chem. 270, 19651–19658.

Lombardo, E., Ramirez, J.C., Garcia, J., Almendral, J.M., 2002. Complementary roles of multiple nuclear targeting signals in the capsid proteins of the parvovirus minute virus of mice during assembly and onset of infection. J. Virol. 76, 7049–7059.

Lorson, C., Pearson, J., Burger, L., Pintel, D.J., 1998. An Sp1-binding site and TATA element are sufficient to support full transactivation by proximally bound NS1 protein of minute virus of mice. Virology 240, 326–337.

Miller, C.L., Pintel, D.J., 2002. Interaction between parvovirus NS2 protein and nuclear export factor Crm1 is important for viral egress from the nucleus of murine cells. J. Virol. 76, 3257–3266.

Mousset, S., Ouadrhiri, Y., Caillet-Fauquet, P., Rommelaere, J., 1994. The cytotoxicity of the autonomous parvovirus minute virus of mice nonstructural proteins in FR3T3 rat cells depends on oncogene expression. J. Virol. 68, 6446–6453.

Muranyi, W., Haas, J., Wagner, M., Krohne, G., Koszinowski, U.H., 2002. Cytomegalovirus recruitment of cellular kinases to dissolve the nuclear lamina. Science 297, 854–857.

Naito, S., Matsumoto, S., 1978. Identification of cellular actin within the rabies virus. Virology 91, 151–163.

Nüesch, J.P., Tattersall, P., 1993. Nuclear targeting of the parvoviral replicator molecule NS1: evidence for self-association prior to nuclear transport. Virology 196, 637–651.

Nüesch, J.P., Corbau, R., Tattersall, P., Rommelaere, J., 1998a. Biochemical activities of minute virus of mice nonstructural protein NS1 are modulated in vitro by the phosphorylation state of the polypeptide. J. Virol. 72, 8002–8012.

Nüesch, J.P., Dettwiler, S., Corbau, R., Rommelaere, J., 1998b. Replicative functions of minute virus of mice NS1 protein are regulated in vitro by phosphorylation through protein kinase C. J. Virol. 72, 9966–9977.

Nüesch, J.P., Christensen, J., Rommelaere, J., 2001. Initiation of minute virus of mice DNA replication is regulated at the level of origin unwinding by atypical protein kinase C phosphorylation of NS1. J. Virol. 75, 5730–5739.

Nüesch, J.P., Lachmann, S., Corbau, R., Rommelaere, J., 2003. Regulation of minute virus of mice NS1 replicative functions by atypical PKC lambda in vivo. J. Virol. 77, 433–442.

Perander, M., Bjorkoy, G., Johansen, T., 2001. Nuclear import and export signals enable rapid nucleocytoplasmic shuttling of the atypical protein kinase C lambda. J. Biol. Chem. 276, 13015–13024.

Pollard, T.D., Blanchoin, L., Mullins, R.D., 2001. Actin dynamics. J. Cell Sci. 114, 3–4.

Pujol, A., Deleu, L., Nüesch, J.P., Cziepluch, C., Jauniaux, J.C., Rommelaere, J., 1997. Inhibition of parvovirus minute virus of mice replication by a peptide involved in the oligomerization of nonstructural protein NS1. J. Virol. 71, 7393–7403.

Ros, C., Kempf, C., 2004. The ubiquitin-proteasome machinery is essential for nuclear translocation of incoming minute virus of mice. Virology 324, 350–360.

Ros, C., Burckhardt, C.J., Kempf, C., 2002. Cytoplasmic trafficking of minute virus of mice: low-pH requirement, routing to late endosomes, and proteasome interaction. J. Virol. 76, 12634–12645.

Sasaki, H., Nakamura, M., Ohno, T., Matsuda, Y., Yuda, Y., Nonomura, Y., 1995. Myosin-actin interaction plays an important role in human immunodeficiency virus type 1 release from host cells. Proc. Natl. Acad. Sci. U.S.A. 92, 2026–2030.

Suikkanen, S., Aaltonen, T., Nevalainen, M., Valilehto, O., Lindholm, L., Vuento, M., Vihinen-Ranta, M., 2003a. Exploitation of microtubule cytoskeleton and dynein during parvoviral traffic toward the nucleus. J. Virol. 77, 10270–10279.

Suikkanen, S., Antila, M., Jaatinen, A., Vihinen-Ranta, M., Vuento, M., 2003b. Release of canine parvovirus from endocytic vesicles. Virology 316, 267–280.

Uberall, F., Hellbert, K., Kampfer, S., Maly, K., Villunger, A., Spitaler, M., Mwanjewe, J., Baier-Bitterlich, G., Baier, G., Grunicke, H.H., 1999. Evidence that atypical protein kinase C-lambda and atypical protein kinase C-zeta participate in Ras-mediated reorganization of the F-actin cytoskeleton. J. Cell Biol. 144, 413–425.

Vihinen-Ranta, M., Yuan, W., Parrish, C.R., 2000. Cytoplasmic trafficking of the canine parvovirus capsid and its role in infection and nuclear transport. J. Virol. 74, 4853–4859.

Vihinen-Ranta, M., Suikkanen, S., Parrish, C.R., 2004. Pathways of cell infection by parvoviruses and adeno-associated viruses. J. Virol. 78, 6709–6714.

Young, P.J., Jensen, K.T., Burger, L.R., Pintel, D.J., Lorson, C.L., 2002a. Minute virus of mice NS1 interacts with the SMN protein, and they colocalize in novel nuclear bodies induced by parvovirus infection. J. Virol. 76, 3892–3904.

Young, P.J., Jensen, K.T., Burger, L.R., Pintel, D.J., Lorson, C.L., 2002b. Minute virus of mice small nonstructural protein NS2 interacts and colocalizes with the Smn protein. J. Virol. 76, 6364–6369.

Zadori, Z., Szelei, J., Lacoste, M.C., Li, Y., Gariepy, S., Raymond, P., Allaire, M., Nabi, I.R., Tijssen, P., 2001. A viral phospholipase A2 is required for parvovirus infectivity. Dev. Cell 1, 291–302.